Semirelativistic technique for k·p calculations: Optical properties of Pd and Pt

E. E. Krasovskii and W. Schattke
Institut für Theoretische Physik, Christian-Albrechts-Universität, Leibnizstrasse 15, D-24098 Kiel, Germany
(Received 9 February 2001; published 24 May 2001)

A semirelativistic two-component extended linear augmented plane-wave $\mathbf{k}\cdot\mathbf{p}$ method is described. In order to ensure a high accuracy of the $\mathbf{k}\cdot\mathbf{p}$ method, it is necessary to include into the radial-basis set, which is used for the augmentation of the plane waves, functions that are neither solutions of the Schrödinger equation nor their energy derivatives. The usual scalar relativistic procedure, which is nonlinear in energy, is not applicable to such basis sets. As an alternative, we suggest an approximation to the Foldy-Wouthuysen Hamiltonian that produces an explicitly Hermitean matrix in the augmented plane wave representation. The technique is applied to the calculation of the full dielectric matrix and optical properties of palladium and platinum metals over the photon energy region up to 100 eV. Special attention is paid to the far ultraviolet absorption by the excitations of semicore Pd $4p$ and Pt $5p$ and $4f$ states. A strong effect of local fields is observed in the far UV region.

DOI: 10.1103/PhysRevB.63.235112 PACS number(s): 71.15.Ap, 78.40.−q, 71.15.Rf

I. INTRODUCTION

Optical properties of metals in the far UV frequency range have been extensively studied experimentally.[1] However, theoretical *ab initio* studies for photon energies above 20 eV are still very rare. It is no straightforward task to generate the band structure in a wide energy range with sufficient accuracy of eigenenergies and wave functions within reasonable computer time. The problem is complicated by the need to compute a full dielectric matrix $\varepsilon_{\mathbf{GG}'}(\omega)$: the microscopic fields generated by the optical excitations of semicore electrons may dramatically change the intensity and shape of the far-UV absorption spectrum.[2] The calculation of the $\varepsilon_{\mathbf{GG}'}$ matrix is very time consuming because it is necessary to evaluate the matrix elements of the $\exp[i\mathbf{Gr}]$ operator for several $\mathbf{G}$ shells. A way to facilitate such calculations is provided by the $\mathbf{k}\cdot\mathbf{p}$ band-structure approach.

The $\mathbf{k}\cdot\mathbf{p}$ formalism reduces the $\mathbf{k}$-point dependence of the basis set to a multiplication of the basis functions with a reference Bloch vector $\mathbf{k}_0$ by the function $\exp[i(\mathbf{k}-\mathbf{k_0})\mathbf{r}]$. The $\mathbf{k}\cdot\mathbf{p}$ formulation is convenient when the functions have sophisticated numerical representation, as, e.g., in the extended linear augmented plane wave (ELAPW) method,[3] because the time-consuming operations of setting up the Hamiltonian, overlap, and momentum matrices are performed only once for a given crystal potential. In calculating the dielectric matrix, we take advantage of the fact that the transfer matrix between the augmented plane wave (APW) and pure plane wave (PW) representation is also $\mathbf{k}$ independent. Having obtained the all-electron eigenfunctions $\psi_n^{\mathbf{k}}$, we change to a PW expansion of $\psi_n^{\mathbf{k}}$ to evaluate the matrix elements $\langle \mathbf{k}m|\exp[i\mathbf{Gr}]|\mathbf{k}n\rangle$.[2]

That the basis set of a $\mathbf{k}\cdot\mathbf{p}$ method is not Bloch-vector adjusted causes the accuracy of the method to deteriorate with the distance $\Delta k=|\mathbf{k}-\mathbf{k_0}|$ from the reference point. The problem is especially severe in the case of localized states, such as semicore states or d states of noble metals. For example, to reproduce an orbital $\Phi_{lm}(\mathbf{r})=\Phi_l(r)Y_{lm}(\hat{\mathbf{r}})$ the trial function has to take the form $\Phi_{lm}(\mathbf{r})\exp[-i(\mathbf{k}-\mathbf{k_0})\mathbf{r}]$, which is an infinite angular momentum series. For a given lm, the number of orbitals is finite, but their radial parts are not solutions of the radial Schrödinger equation. Such orbitals do not cause any inconveniences in nonrelativistic calculations, where the properties of the Hamiltonian $-\Delta+V(\mathbf{r})$ are simple and the energy variation principle is clearly formulated, but in the relativistic case the inclusion of such orbitals is not straightforward.

In band structure calculations, relativistic effects can be taken into account either within the fully-relativistic four-component procedure,[4–6] in which no approximations to the Hamiltonian are introduced, or by a semirelativistic two-component technique.[7–9] The latter approach has the advantage that the basis functions can be chosen to be pure spin functions, which may be useful in magnetic calculations; in addition, in many cases the spin-orbit coupling can be omitted—this leads to one-component (scalar) functions and strongly reduces the computer time.

In the linear methods of band theory,[10] the scalar relativistic corrections are routinely included using the technique of Koelling and Harmon (KH).[7] The radial functions $\phi_l(r)$ are the solutions of the equation

$$(\hat{H}_r-E)\phi_l(r)=0, \tag{1}$$

$$\hat{H}_r=-\frac{1}{r}\frac{d^2}{dr^2}r+\frac{l(l+1)}{r^2}+V(r)-H_{\mathrm{R}}(E), \tag{2}$$

where the relativistic term $H_{\mathrm{R}}(E)$ depends explicitly on the energy E chosen in advance:

$$H_{\mathrm{R}}(E)=\frac{1}{2c^2M(r;E)}\frac{dV}{dr}\frac{d}{dr}+\frac{[E-V(r)]^2}{c^2}, \tag{3}$$

$$M(r;E)=m+\frac{E-V(r)}{2c^2}. \tag{4}$$

With the functions ϕ one has a simple rule for energy integrals: $\langle\xi|\hat{H}|\phi\rangle=E\langle\xi|\phi\rangle$. What values should be ascribed to

integrals $\langle \xi|\hat{H}|\eta\rangle$ with arbitrary orbitals ξ and η? This problem arises in any variational method that employs a fixed basis set. One aim of this paper is to develop a semirelativistic band structure technique that is based on an explicit expression for the Hamiltonian and can thereby be used in a $\mathbf{k}\cdot\mathbf{p}$ method.

An approximate Hamiltonian that operates on two-component wave functions can be obtained by a unitary Foldy-Wouthuysen (FW) transformation[11] on the relativistic Hamiltonian. The (scalar) FW Hamiltonian reads

$$\hat{\mathbf{p}}^2+V(\mathbf{r})-\frac{\alpha^2}{4}\hat{\mathbf{p}}^4+\frac{\alpha^2}{8}[\Delta V(\mathbf{r})], \tag{5}$$

where $\hat{\mathbf{p}}=-i\boldsymbol{\nabla}$ is the momentum operator and $\alpha=2/c$ is the fine structure constant. This expression cannot be immediately used in a direct variational method because the expectation values of the mass-velocity term $-\alpha^2\hat{\mathbf{p}}^4/4$ are not bounded from below. An additional problem arises from the nucleus contribution to the Darwin term $\alpha^2\Delta V(\mathbf{r})/8$: for a point nucleus it is a δ-function.

Douglas and Kroll[12] suggested an alternative transformation, which leads to a Hamiltonian that is bounded from below and does not contain singular operators. The Hamiltonian has a relatively simple momentum-space representation, and when an orbital basis set is employed the matrix elements can be evaluated by switching to a new representation that diagonalizes the kinetic-energy matrix. This approach was proposed by Hess,[13] who implemented it in the Gaussian-type-orbitals (GTO) method and applied it to atomic calculations. Recently Boettger[9] extended the procedure to band structure calculations.

An attempt to use a Foldy-Wouthuysen-type Hamiltonian in a band structure calculation has been made by Fehrenbach and Schmidt,[8] who developed a semirelativistic procedure for the spline APW (SAPW) method.[14] The SAPW basis set includes both plane waves and potential-independent orbitals, whose radial parts are spline functions. To avoid the unbounded matrix elements of the mass-velocity term, the authors replaced the combination $\hat{\mathbf{p}}^2-\alpha^2\hat{\mathbf{p}}^4/4$ with the positive definite operator

$$\frac{2}{\alpha^2}(\sqrt{1+\alpha^2\hat{\mathbf{p}}^2}-1). \tag{6}$$

A direct application of the operator would require a convergent expansion of the basis functions in terms of eigenfunctions of the kinetic-energy operator. Similarly to the method of Hess,[13] the authors change to a new radial-basis set that diagonalizes the operator $\hat{\mathbf{p}}^2$ in the subspace of spline-radial functions.

In contrast to GTO or SAPW methods, the strategy in the linear methods is to include only a small number of potential-adjusted radial basis functions, namely, the solutions of Eq. (1) and their energy derivatives. Routine calculations are performed with 2–4 functions per angular momentum channel—compare with 33–65 spline functions in the SAPW. With their modest radial basis sets the linear methods cannot provide a decent approximation to the kinetic energy eigenfunctions (i.e., Bessel functions), which calls for a technique that does not involve a $\hat{\mathbf{p}}^2$ diagonalization scheme. At the same time, in view of the limited variational freedom inside the atomic sphere, one can avoid the problem of the unbounded $\hat{\mathbf{p}}^2$ operator by restricting the relativistic corrections to the interior of the atomic spheres.

In Sec. II, our approximation to the Foldy-Wouthuysen Hamiltonian is presented and compared to the method of Fehrenbach and Schmidt. We describe the radial basis set of the ELAPW $\mathbf{k}\cdot\mathbf{p}$ method in Sec. III. The computational parameters of the band structure and dielectric matrix calculations are presented in Sec. IV. Optical properties of Pd and Pt in a wide photon energy region are discussed in Sec. V.

II. SEMIRELATIVISTIC HAMILTONIAN

In order to restrict the effect of the mass-velocity term to the interior of the atomic spheres and at the same time keep the Hamiltonian matrix Hermitean, we replace the operator $\hat{\mathbf{p}}^4$ with a ''screened'' operator

$$\hat{\mathbf{p}}^4\rightarrow\chi(r)\hat{\mathbf{p}}^4\chi(r). \tag{7}$$

Here $\chi(r)$ is a smooth function that equals unity at $r=0$ and vanishes with its derivative at the sphere radius S. In actual calculations, the screening function $\chi(r)$ was equal to unity within a sphere of radius $R_0=0.7S$, which is about 1 Å, and, for $r>R_0$, it was

$$\chi(r)=1-\frac{1}{4}\left[\cos\left(\frac{r-R_0}{S-R_0}\pi\right)-1\right]^2.$$

We would like to use the solutions of Eq. (1) as radial basis functions also for $l=0$, in which case the functions diverge as $r^{-Z^2\alpha^2/2}$ with $r\rightarrow 0$ (here Z is the atomic number). This causes a problem in treating the singular nucleus contribution to the Darwin term. We circumvent the difficulty by introducing a finite radius of the nucleus. The radius is determined by the condition that for a given energy E the expectation value of our Hamiltonian for the solution of Eq. (1) coincide with this energy. Then we use the same radius for all functions. The results are practically independent of the choice of the energy E; usually we choose it in the valence-band energy region.

To appraise the quality of the modified FW Hamiltonian we have calculated the scalar relativistic energies of the core states of Ag using the traditional radial basis set of the LAPW method[10] so that the deviations from the energies obtained with the Koelling-Harmon technique[7] stem solely from the inaccuracy of the Hamiltonian. In Table I we compare our results to those of Fehrenbach and Schmidt[8] obtained with the SAPW method. To understand the differences between LAPW and SAPW we compare also the nonrelativistic energies (the first two columns). Here the Hamiltonian is just $\hat{\mathbf{p}}^2+V(\mathbf{r})$, and the energy deviations (from the exact scalar relativistic energies) in SAPW are overestimated by 2–10% in comparison to the LAPW results. This is apparently due to the variational character of

TABLE I. Semirelativistic and nonrelativistic energies of some core states of Ag by the SAPW (Ref. 8) and LAPW methods. Presented are the differences (in Ryd) between the exact scalar relativistic (Koelling-Harmon) energies and those obtained with the nonrelativistic Hamiltonian (subscript N) or a Foldy-Wouthuysen-like Hamiltonian (subscript FW). In the latter case, SAPW employs the expression (6) for the mass-velocity term, and LAPW the approximation (7). In LAPW, for a given Hamiltonian, one can choose radial basis functions in two different ways: the FW results are shown for both the nonrelativistic functions (superscript N) and the scalar relativistic ones (superscript R). The columns $\Delta\dot{E}^{\mathrm{R}}_{\mathrm{FW}}$ and $\Delta\dot{E}^{\mathrm{N}}_{\mathrm{FW}}$ show the expectation values of the energy derivative functions $\dot{\phi}_{\nu l}$, see Eq. (9).

	SAPW ΔE_N	LAPW ΔE_N	SAPW ΔE_{FW}	LAPW $\Delta E^{\mathrm{R}}_{\mathrm{FW}}$	LAPW $\Delta E^{\mathrm{N}}_{\mathrm{FW}}$	LAPW $\Delta\dot{E}^{\mathrm{R}}_{\mathrm{FW}}$	LAPW $\Delta\dot{E}^{\mathrm{N}}_{\mathrm{FW}}$
$2p$	7.248	6.798	0.495	-0.146	0.183	0.357	6.499
$3s$	3.581	3.510	-4.650	0.000[a]	0.348	0.024	3.503
$3p$	1.675	1.570	-0.089	-0.044	0.046	0.013	1.563
$3d$	0.392	0.378	-0.079	-0.006	0.001	0.001	0.371
$4s$	0.710	0.689	-0.903	0.000[a]	0.072	0.000	0.676
$4p$	0.305	0.273	-0.014	-0.008	0.009	-0.001	0.257

[a]The nucleus radius was determined for that energy.

the SAPW radial functions: with only 33–65 spline basis functions the asymptotics at $r\to 0$ seems to be not accurate enough.

The next two columns compare two versions of the semirelativistic Hamiltonian, namely, the LAPW results based on the approximation (7) and their SAPW counterparts obtained with the operator (6). The errors by the two methods are of the same order of magnitude—except for s states, for which the method of Fehrenbach and Schmidt is not applicable. The problem with s states is caused by the failure of the variational procedure to correctly treat the δ function coming from the Darwin term. It should be noted, that the δ function can be straightforwardly included into the Hamiltonian if the basis set is composed of nonrelativistic radial solutions, which are finite at the nucleus. This approximation gives much better results than the SAPW, as one can see from the fifth column, $\Delta E^{\mathrm{N}}_{\mathrm{FW}}$.

At first glance, using nonrelativistic radial solutions instead of scalar relativistic ones, does not actually lower the quality of results: the errors $\Delta E^{\mathrm{N}}_{\mathrm{FW}}$ and $\Delta E^{\mathrm{R}}_{\mathrm{FW}}$ are close in magnitude, but have opposite sign. However, it is important to have relativistic solutions for the energy derivative functions $\dot{\phi}$. The function $\dot{\phi}_l$ satisfies the equations

$$(\hat{H}_r - E)\,\dot{\phi}_l(r) = \phi_l(r), \quad \langle \phi_l | \dot{\phi}_l \rangle = 0, \tag{8}$$

and its energy expectation value is equal to E

$$E - \frac{\langle \dot{\phi}_l | \hat{H}_r | \dot{\phi}_l \rangle}{\langle \dot{\phi}_l | \dot{\phi}_l \rangle} = \Delta\dot{E} = 0. \tag{9}$$

The last two columns demonstrate that when the operator $\hat{H}_r$ is taken to be the FW Hamiltonian this equation is fulfilled with a good accuracy for relativistic $\dot{\phi}$, but not for the nonrelativistic ones. Indeed, the atomiclike states decay as $\exp(-r\sqrt{-E})/r$ for large r, and the function $\dot{\phi}_{\nu l}$, which asymptotically obeys the equation $(\hat{H}_r - E)\,\dot{\phi}_{\nu l} = 0$, grows as $\exp(r\sqrt{-E})/r$. Thus, far from the nucleus the nonrelativistic $\dot{\phi}_{\nu l}$ function differs from the relativistic one just because the energy E is different, and it is the large radii that give the dominant contribution to the energy integral (see Fig. 1). The $\Delta\dot{E}^{\mathrm{N}}_{\mathrm{FW}}$ values are seen to be very close to those in the ΔE_{N} column, which reflects the ''short-range'' character of the relativistic corrections.

Owing to the neglect of the terms of higher order in α in the FW Hamiltonian (5), the error grows with increasing the atomic number. Apart from that, an error is introduced in treating the spin-orbit coupling when the dependence of the radial functions upon the quantum number κ is neglected,[15] i.e., the so-called second-variational treatment is adopted. We include the spin-orbit interaction only inside the atomic spheres in the form derived by Koelling and Harmon[7]

$$\frac{1}{[2cM(r;E)]^2}\,\frac{1}{r}\,\frac{dV(r)}{dr}\hat{\boldsymbol{\sigma}}\cdot\hat{\mathbf{L}}, \tag{10}$$

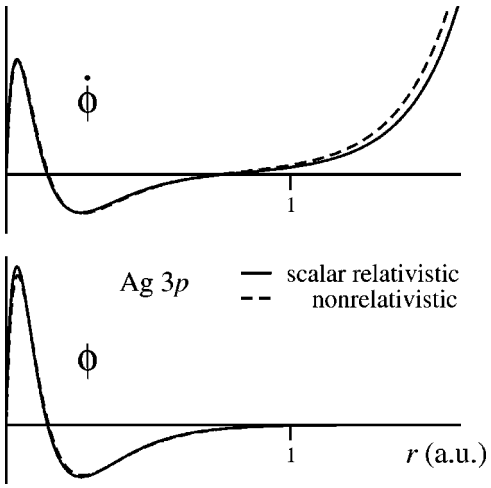

FIG. 1. Scalar relativistic and nonrelativistic $3p$ radial functions of Ag.

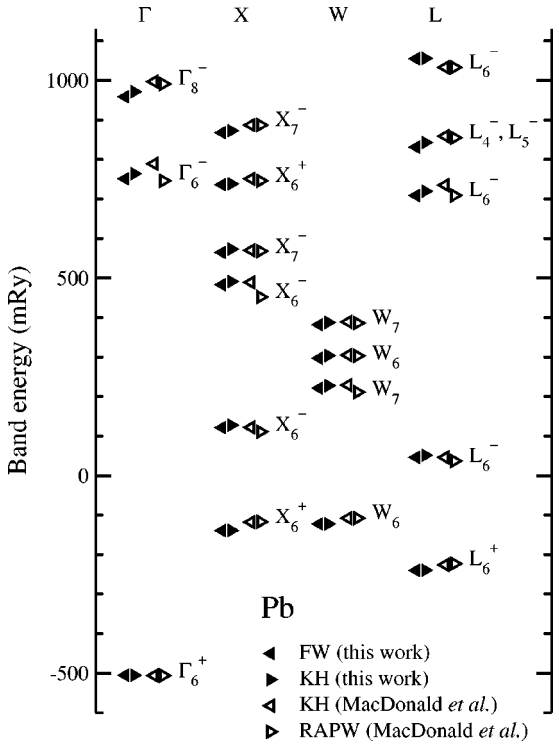

FIG. 2. Comparison of the band energies for fcc Pb obtained with the FW-type Hamiltonian (full triangles left) to those by the KH technique with the same basis set (full triangles right) and to the results of MacDonald *et al*. (Ref. 15) by the KH technique (open triangles left) and by the relativistic APW (open triangles right).

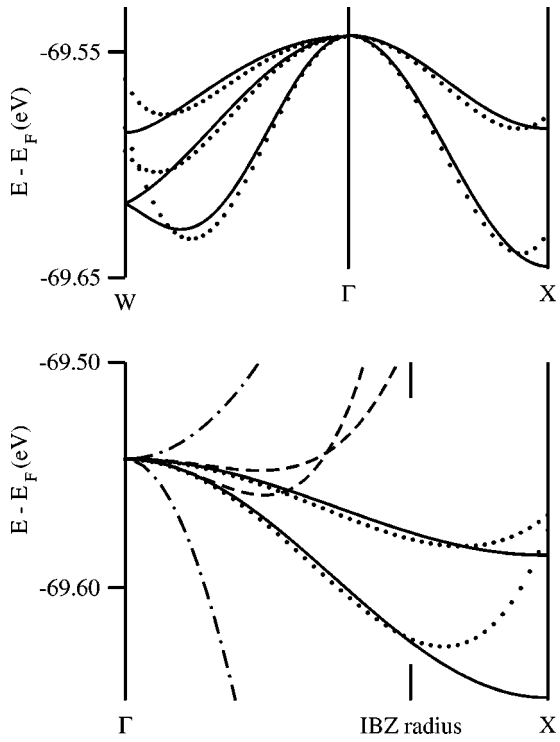

FIG. 3. Scalar relativistic $3p$ bands of Cu. Solid lines show the exact ELAPW $E(\mathbf{k})$ curves. In the $\mathbf{k}\cdot\mathbf{p}$ calculations the reference point $\mathbf{k_0}$ is at Γ. In the lower panel the dot-dashed lines show an attempt to solve the $\mathbf{k}\cdot\mathbf{p}$ problem with only ϕ and $\dot{\phi}$ functions, namely the radial solutions with the number of nodes from 1 to 7 for *s*, from 0 to 6 for *p* and for *d*, and from 0 to 4 for *f* functions. One $\dot{\phi}$ function per *l* channel was included. The dashed lines present the ELAPW-$\mathbf{k}\cdot\mathbf{p}$ results with only the functions of the first order in Δk, $\Phi_{l=1}(r)rY^m_{l\pm1}(\hat{\mathbf{r}})$, added to the minimal basis set (i.e., to the traditional ϕ and $\dot{\phi}$ pairs, see Ref. 10). Extending the set by the second-order functions, $\Phi_{l=1}(r)r^2Y^m_l(\hat{\mathbf{r}})$ and $\Phi_{l=1}(r)r^2Y^m_{l\pm2}(\hat{\mathbf{r}})$, results in the dotted lines. The two bars in the lower panel show the distance from the center of gravity of the fcc IBZ to its most remote point (point Γ). In the upper panel, the dotted curves result from a calculation in which the radial basis set was further extended by ϕ functions to take into account corrections of order higher than second in Δk.

the relativistic mass $M(r;E)$ [see Eq. (4)] being energy independent in our calculations and taken at $E=0$.

In Fig. 2 we compare band energies of the fcc Pb calculated with our version of the FW Hamiltonian to our KH results and to the LAPW-KH and relativistic APW (RAPW) energies of MacDonald *et al.*[15] The errors due to our semirelativistic approximation do not exceed 15 mRy; they are smaller than the discrepancies between the KH results of the present work and of MacDonald *et al*., which are apparently caused by the differences in crystal potential and in basis set. The $p_{1/2}$ states are known to suffer stronger than the $p_{3/2}$ states from the neglect of the κ dependence of the radial function,[15] compare, e.g., Γ_6^- and Γ_8^- energies in LAPW and RAPW. Again, this error is seen to be larger than the inaccuracy of the FW approximation. For *d* states of $5d$ metals, the errors are smaller (within 10 mRy), which is to be expected as the *d* electrons do not approach the nucleus as closely as the *p* electrons do.

We infer from the above discussion that the approximation to the Foldy-Wouthuysen Hamiltonian that involves the ''screening'' of the mass-velocity term, Eq. (7), and the finite nucleus radius for the divergent *s* radial functions is sufficiently accurate to be used in spectroscopic calculations.

III. RADIAL SET OF THE ELAPW-k·p METHOD

The $\mathbf{k}\cdot\mathbf{p}$ representation of the orbital $\Phi_{lm}(\mathbf{r})$ is $\Phi_{lm}(\mathbf{r})\exp[-i(\mathbf{k}-\mathbf{k_0})\mathbf{r}]$. Let us perform the angular momentum decomposition of the factor $\exp[i\Delta\mathbf{kr}]$, expand the Bessel functions into the Taylor series of the argument Δkr, and keep only the radial functions proportional to the first and second power of Δk. This brings five new types of orbitals to be included in constructing the trial function, namely two orbitals of the first order in Δk, $\Phi_l(r)rY^m_{l\pm1}(\hat{\mathbf{r}})$, and three orbitals of the second order, $\Phi_l(r)r^2Y^m_l(\hat{\mathbf{r}})$ and $\Phi_l(r)r^2Y^m_{l\pm2}(\hat{\mathbf{r}})$. The orbitals we intend to reproduce are close to linear combinations of $\phi_{\nu l}$ and $\dot{\phi}_{\nu l}$, so we include both $\Phi_l=\phi_{\nu l}$ and $\Phi_l=\dot{\phi}_{\nu l}$ orbitals.

Figure 3 illustrates the effect of the functions of the first and the second order in Δk on the quality of the semicore $3p$ states of Cu. The inclusion of the functions up to the second order provides an acceptable accuracy within the Δk radius of $0.7(2\pi/a)$ (dotted curves), i.e., the entire irreducible Bril-

TABLE II. Energy parameters and radial basis set of the ELAPW-$\mathbf{k}\cdot\mathbf{p}$ method for Pt. The radial functions are arranged in pairs; each one (except for the second *s* pair) comprises a solution ϕ and its energy derivative $\dot{\phi}$, which describe one logarithmic derivative branch. [10] The Pt $6s$ branch is rather narrow, so we had to include also the $7s$ one in order to describe the required energy region. Energies are given in Rydbergs relative to the muffin-tin zero.

	$l=0$	$l=1$	$l=2$	$l=3$	$l=4$
E_ν^{I}	$E_{5s}=-6.59$	$E_{5p}=-3.24$	$E_{5d}=0.45$	$E_{4f}=-4.26$	$E_{5g}=3.47$
E_ν^{II}	$E_{6s}=0.30$	$E_{6p}=1.71$	$E_{6d}=4.25$	$E_{5f}=3.47$	
E_ν^{III}	$E_{7s}=6.52$				
1st pair	$\phi_{5s},\dot{\phi}_{5s}$	$\phi_{5p},\dot{\phi}_{5p}$	$\phi_{5d},\dot{\phi}_{5d}$	$\phi_{4f},\dot{\phi}_{4f}$	$\phi_{5g},\dot{\phi}_{5g}$
2nd pair	ϕ_{6s},ϕ_{7s}	$\phi_{6p},\dot{\phi}_{6p}$	$\phi_{6d},\dot{\phi}_{6d}$	$\phi_{5f},\dot{\phi}_{5f}$	$\phi_{5f},\dot{\phi}_{5f}\cdot r$
3rd pair	$\phi_{5p},\dot{\phi}_{5p}\cdot r$	$\phi_{5d},\dot{\phi}_{5d}\cdot r$	$\phi_{5f},\dot{\phi}_{5f}\cdot r$	$\phi_{5d},\dot{\phi}_{5d}\cdot r$	
4th pair		$\phi_{5p},\dot{\phi}_{5p}\cdot r^2$			

louin zone (IBZ) is covered if the reference point is placed in its center of gravity.

In the original formulation of the ELAPW-$\mathbf{k}\cdot\mathbf{p}$ method,[3] the idea was to take advantage of the fact that the functions $\Phi_l r^N$ can be expanded in a convergent series of the radial solutions $\phi_{\nu l'}$ for a given l'. (Indeed, the functions $\phi_{\nu l'}$ with the same logarithmic derivative $D_{l'}$ are eigenfunctions of a Hermitean operator, and a function with a different logarithmic derivative, e.g., $\dot{\phi}_{\nu l'}$ must be added to the set to bring the function $\Phi_l r^N$ to that Hilbert space.) With a small number of functions $\phi_{\nu l'}$ and $\dot{\phi}_{\nu l'}$ the quality was satisfactory for the extended states of the conduction band,[3] however, for semicore states or the *d* states of noble metals the series converges very slowly. In practice, the accuracy cannot be further increased by merely extending the radial basis set with more $\phi_{\nu l'}$, which is demonstrated by the dot-dashed curves in Fig. 3.

Our experience shows that for valence-band states—even in transition and noble metals—it is necessary to include only the functions of the first order in Δk, and the higher-order corrections can be performed by extra ϕ and $\dot{\phi}$ functions. Extra radial solutions are anyway present in wide energy range calculations because several logarithmic derivative branches[10] are to be described.

IV. COMPUTATIONAL METHODOLOGY

The self-consistent potential of Pd and Pt metals was constructed within the local density approximation (LDA) of the density functional theory with the full-potential augmented Fourier components technique described in Ref. 16. The Kohn-Sham equations were solved with the ELAPW-$\mathbf{k}\cdot\mathbf{p}$ method. The basis set included 89 energy-independent APW's (energy cutoff 13.7 Ry), and the extension of the radial basis set contributed another 98 basis functions. The extension was introduced following the prescriptions of the preceding section; an example of the radial basis set for Pt is presented in Table II. The Brillouin zone (BZ) integrations were performed by the tetrahedron method with a mesh of 413 $\mathbf{k}$ points that divides the BZ into 82 944 tetrahedra, 1864 of which are inequivalent.

The dielectric matrix was calculated in the framework of the random phase approximation (RPA),[17,18] the effects of exchange and correlation (XC) in the induced fields were taken into account within the time-dependent adiabatic LDA (TDLDA).[19] The matrix elements of the $\exp[i\mathbf{G}\mathbf{r}]$ operator were calculated using a decomposition of the all-electron wave functions into 11 935 plane waves. A detailed description of the methodology can be found in Ref. 2. The $\varepsilon_{\mathbf{G}\mathbf{G}'}(\omega)$ matrix was computed for five coordination shells (51 $\mathbf{G}$ vectors). The real parts of the matrix elements were determined out of their imaginary parts by the Kramers-Kronig integration with the energy cutoff $\hbar\omega_{\max}=150$ eV (60 bands in the unoccupied part of the energy spectrum had to be considered).

As expected, owing to the neglect of the κ dependence of the radial functions, the spin-orbit splitting of semicore *p* bands was considerably underestimated: it was 4.3 eV for Pd $4p$ and 13.5 eV for Pt $5p$ states, whereas the fully relativistic atomic calculations give 4.5 and 15.0 eV, respectively. The splitting of Pt $4f$ states was reproduced with a better accuracy: 3.40 eV instead of 3.46 eV in the atomic calculation. We considered the Pd $4p$ and Pt $4f$ errors tolerable, but in the case of Pt $5p$, we had to interfere: at the stage of calculating the spectral functions we shifted the $5p_{1/2}$ band by 1.2 eV to lower energies and the $5p_{3/2}$ by 0.3 eV to higher energies in order to bring their positions relative to the $4f_{5/2}$ and $4f_{7/2}$ bands in agreement with the fully relativistic calculation for a free atom.

V. OPTICAL PROPERTIES OF Pd AND Pt

Let us first consider the photon energy range below the absorption edges of the semicore *p* states. The *ab initio* macroscopic dielectric function $\varepsilon(\omega)$ as well as the normal incidence reflectivity and the electron-energy-loss spectra (EELS) for Pd and Pt are shown in Figs. 4 and 5, respectively. The optical spectra are compared to the results derived by Weaver *et al.*[1] from different measurements; the dots in both figures are taken from the tabulation in Ref. 1.

As in our previous calculation[2] for Nb we do not observe a strong effect of local fields below the semicore excitation energies. Only in the EELS spectrum, which is very sensitive

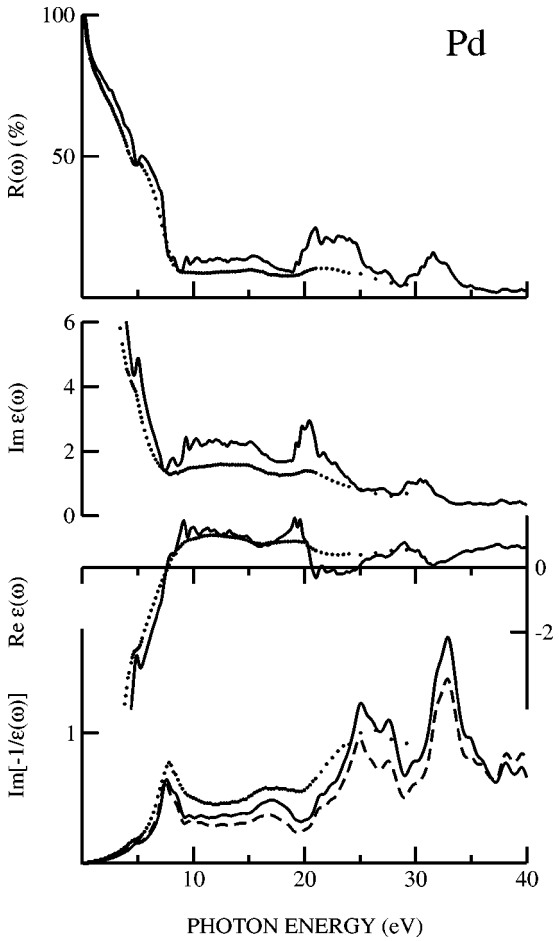

FIG. 4. Reflectivity $R(\omega)$, macroscopic dielectric function $\varepsilon(\omega)$, and loss function $\mathrm{Im}[-\varepsilon(\omega)^{-1}]$ of Pd. Solid lines: theory, dashed line: theoretical loss function with local field effects neglected, dots: experiment of Ref. 1.

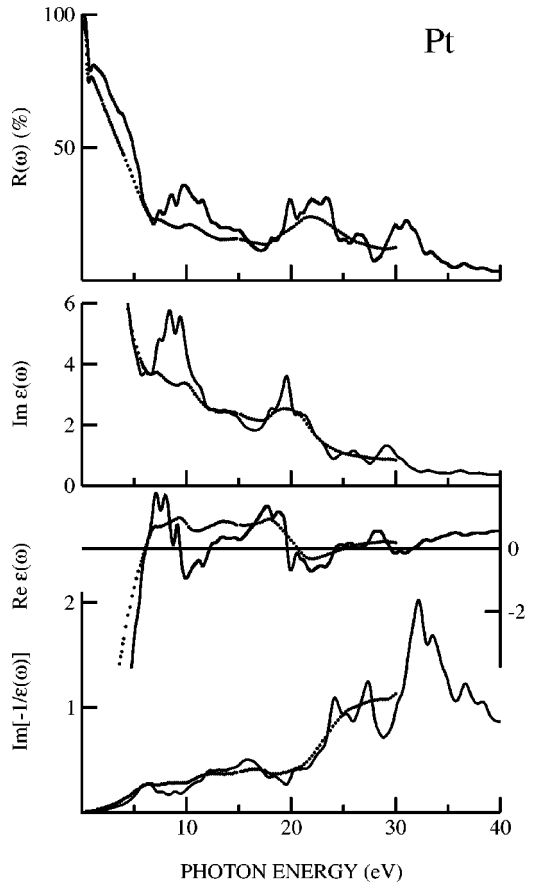

FIG. 5. Reflectivity $R(\omega)$, macroscopic dielectric function $\varepsilon(\omega)$, and loss function $\mathrm{Im}[-\varepsilon(\omega)^{-1}]$ of Pt. Solid lines: theory, dots: experiment of Ref. 1.

to small variations of the dielectric function, the effect is visible. In the lowermost panel of Fig. 4 we show also the spectrum without the local field effects, i.e., the Im $[-\varepsilon_{00}(\omega)^{-1}]$ curve (dashed line). The peak positions are seen to remain unchanged, but the difference in intensity steadily grows with increasing the energy.

We did not observe any tangible effect of the spin-orbit coupling on the spectra of both Pd and Pt below 40 eV. Our calculations are in excellent agreement with available optical data,[20–23] and they do not reveal any inadequacy of the one-electron approach—the discrepancies between theory and experiment seem to be within the experimental uncertainty. The positions of the theoretical EELS maxima agree satisfactory with the energy-loss measurements discussed in Ref. 24, but above 10 eV the intensity and overall shapes of the spectra rather disagree: calculated EELS of Pd and Pt are similar, whereas their measured counterparts are very different.

It should be kept in mind that apart from the approximate RPA-TDLDA treatment of the exchange and correlation, our calculation, as well as the majority of the state-of-the-art calculations, suffer from the neglect of many-body effects in the band structure itself. A correct (quasiparticle) band structure would have resulted from a one-particle equation that includes the many-body effects through the exact self-energy operator $\hat{\Sigma}$,[25]

$$[\hat{H}_1+\hat{\Sigma}(E)]|\psi\rangle=E|\psi\rangle, \tag{11}$$

where $\hat{H}_1$ describes the kinetic energy and Coulomb interaction, and the operator $\hat{\Sigma}$ is, in general, energy dependent, nonlocal, and not Hermitian. In our calculations, $\hat{\Sigma}$ is replaced with a local exchange-correlation potential $v_{xc}(\mathbf{r})$ obtained within the LDA. At the present-day level of the many-body theory it is not possible to *a priori* estimate the error of the simplified one-electron calculations, and the comparison with the experiment remains the main argument in judging on the adequacy of approximations. It is therefore important that the *ab initio* results be produced with numerical accuracy high enough to reveal the limitations of the theory and that the parameters affecting the peak positions and intensities be clearly understood.

In this respect, a recent study of the EELS of Pd by Fehrenbach[26] needs to be commented on. The spectrum for $\hbar\omega<30$ eV was obtained with the SAPW method and a mixed basis representation of the inverse dielectric matrix

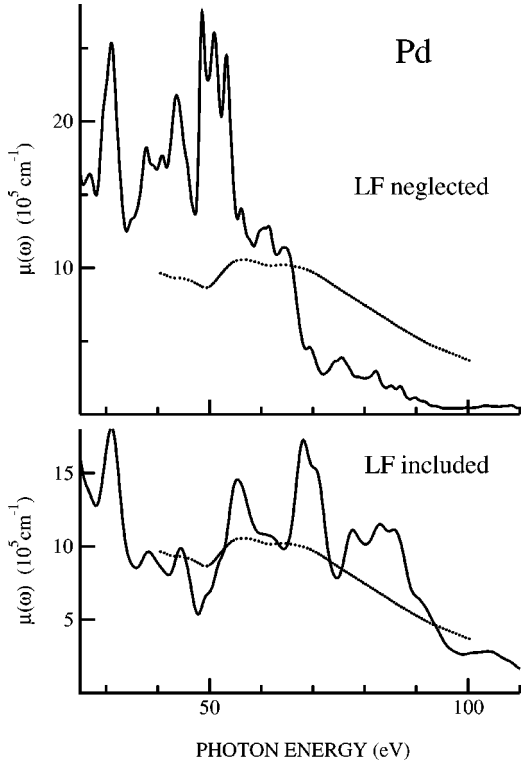

FIG. 6. Absorption coefficient of Pd. Solid lines: theory, dotted line: experiment of Weaver and Olson (Ref. 23).

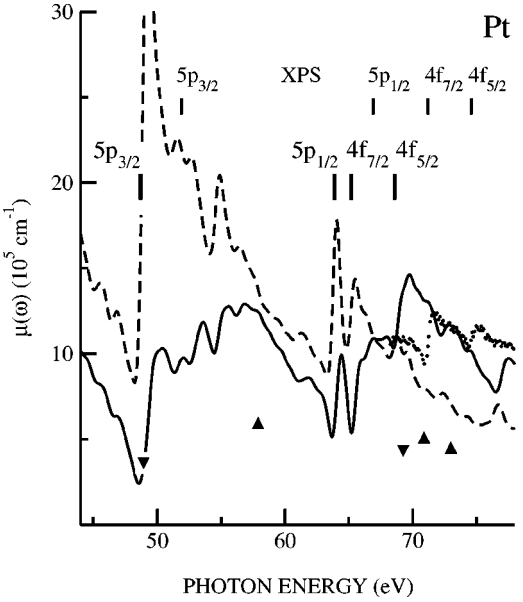

FIG. 7. Absorption coefficient of Pt with (solid line) and without (dashed line) local field effects. Dots are the experiment of Dietz *et al.* (Ref. 31). Triangles show the positions and relative magnitude of maxima (triangles up) and minima (triangles down) in the experiment of Haensel *et al.* (Ref. 30). (The triangles are shifted downwards by 5×10^5 cm^{-1} to avoid the overlap with the other curves in the picture.) Longer bars show the LDA-derived energies of the semicore bands, and shorter bars the XPS results of Wertheim and Walker (Ref. 32) and Wertheim (Ref. 33).

was used. It is claimed in Ref. 26 that ''even at low frequencies it is necessary to include a large part of the spectrum . . . in order to describe the structure of EELS correctly.'' In that work 500 conduction bands were included (energy cutoff of several hundred Rydbergs) and the work by Mazin *et al.*[27] was criticized for using only 16 valence and conduction bands. Our experience does not support that conclusion. The energy cutoff corresponding to the 16 band is about 45 eV, so the contribution from the omitted part of the spectrum to the Kramers-Kronig integrals for $\hbar\omega<30$ eV is a slowly varying function and it does not strongly affect the peak positions. Moreover, in our 16-band calculation for Pd also the intensity of the Im$[-\varepsilon_{00}(\omega)^{-1}]$ spectrum changed only slightly, so that the ''underconverged'' curve lied between the solid and the dashed lines in the lowermost panel of Fig. 4.

The majority of the measurements locate the low-energy plasmon peak in Pd near 7.6 eV (Refs. 1,20,21,24)—in perfect agreement with our calculations. The nonrelativistic calculations by Fehrenbach[26] and by Maksimov and co-workers[27,28] [with the linear muffin-tin orbitals method (LMTO)] give the plasmon energy at 8.2 and 8.4 eV, respectively. The theoretical EELS curves of Refs. 26 and 28 are in poor agreement with available experiments.[29] In Ref. 26 many-body effects or relativistic corrections not included in the calculations were suggested as a possible source of the disagreement. According to our calculations, a complete exclusion of relativistic effects does not strongly change the EELS curve: the plasmon moves from 7.6 to 7.9 eV and the maximum at 17 eV becomes less pronounced. We conclude that both of the previous calculations suffered from a lack of numerical accuracy. In LMTO the main problem is known to come from the small basis set, which is especially inefficient in the interstitial region, and in SAPW it apparently comes from the variational character of the radial functions (see the discussion in Sec. II).

Optical data for far-UV frequency range—the absorption coefficient $\mu(\omega)$—are shown in Figs. 6 and 7 for Pd and Pt, respectively. The figures illustrate the strong effect of the nondiagonal dielectric response[18] on the optical absorption by semicore excitations. In Pd, the local fields redistribute the absorption intensity of the transitions from the $4p_{1/2}$ (binding energy 52.7 eV) and $4p_{3/2}$ states (48.4 eV) into two maxima at 55.5 and 69 eV—in a satisfactory agreement with the measurements by Weaver and Olson.[23] For Pd, the relativistic splitting of the $4p$ band has proved unimportant: owing to the absence of narrow final-state bands, the widths of the $4p_{1/2}$ and $4p_{3/2}$ partial contributions to the $\varepsilon_{\mathbf{GG}'}(\omega)$ curves are much larger than their spin-orbit splitting.

In both Pd and Pt, the shape of the $\mu(\omega)$ curves on a large energy scale is determined by the $p_{3/2}$ excitations. The Pt $5p_{3/2}$ binding energy in our calculation was 48.7 eV—very close to the Pd $4p_{3/2}$ energy of 48.4 eV. Because of that, the spectra between 40 and 100 eV are rather similar. In contrast to the measurements on Pd,[23] the experimental $\mu(\omega)$ data[30,31] on Pt resolve an interesting double structure around 72 eV. The shape of the structure is determined by the overlapping contributions from $5p_{1/2}$, $4f_{5/2}$, and $4f_{7/2}$ bands (the

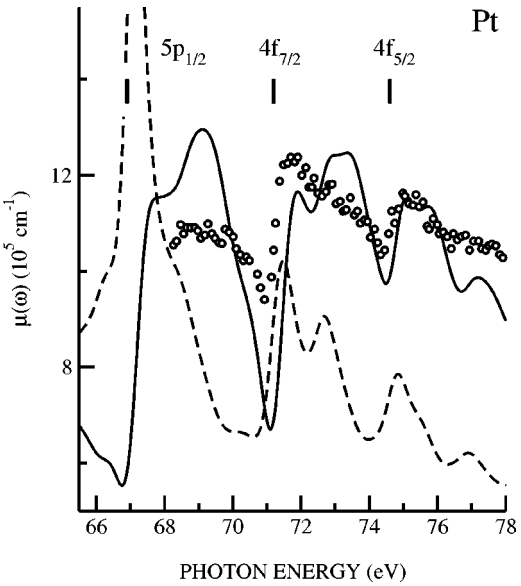

FIG. 8. Absorption coefficient of Pt calculated with the energies of the semicore bands changed so as to agree with the XPS data of Refs. 32 and 33 (shown by vertical bars). Solid line is theory with and dashed line without local fields. Circles are the experiment of Dietz *et al.* (Ref. 31).

energy location of the bands in our calculation is shown by longer bars in Fig. 7). Although the energy location and the separation of the two peaks around 72 eV in the measurements by Haensel *et al.*[30] (triangles in Fig. 7) and by Dietz *et al.*[31] (dots) disagree by 0.5–1 eV, they both agree in that the experimental structures—especially the minima—are much more pronounced than in our calculations.

Presumably, we are here confronted with the many-body effects not included in our calculations. It should be noted that our calculated binding energies are in disagreement with the values derived from x-ray photoelectron spectroscopy (XPS) measurements by Wertheim and Walker[32] for Pt $4f_{7/2}$ and $4f_{5/2}$ bands, 71.2 and 74.6 eV, and by Wertheim[33] for $5p_{3/2}$ and $5p_{1/2}$ bands, 51.9 and 66.9 eV. The XPS data are displayed in Fig. 7 by shorter bars. Although the experimental binding energies cannot be directly associated with the one-particle energies entering the RPA expression[18] for the dielectric matrix, the deviations of the LDA energies from the XPS data give the order of magnitude of the theoretical uncertainty. It is interesting to study the effect of such corrections on the absorption spectra. We have recalculated the $\mu(\omega)$ curve with the energies of the semicore states changed so as to coincide with the XPS data. As can be expected the result is that the minimum at 49 eV moves to higher energies away from its measured position. On the other hand, the situation around 72 eV considerably improves: the minima acquire the experimentally observed sharpness and the shape and energy location of the double structure now perfectly accord with the experiment of Dietz *et al.*[31] (see Fig. 8).

One can see that by manipulating the band energies of the localized states one can bring the theoretical spectrum to a rather close agreement with experiment over the entire high-energy spectral range. Most important is that cannot be achieved without taking into account the local field effects: compare the solid and the dashed curves in Fig. 8. The discrepancies between the *ab initio* theory (Fig. 7) and the experiment can be ascribed to the LDA potential being employed as a self-energy operator, Eq. (11). However, since it only causes rigid band shifts, the XC potential of the LDA appears to be a plausible first guess for the self-energy. It is possible that a more accurate prescription for the XC operator, which would exclude the electron self-interaction,[34] would lead to a semicore band structure more appropriate also for optical properties. Indeed, the more localized the states the stronger the self-interaction corrections, and in our case one can expect the $4f$ states to be more strongly shifted from their LDA positions than the $5p$ states—that sort of correction might be needed to reproduce the experiment.

VI. CONCLUSIONS

The inclusion of radial functions coming from the product $\Phi_{lm}(\mathbf{r})\exp[-i(\mathbf{k}-\mathbf{k_0})\mathbf{r}]$ into the basis set of the ELPAW-$\mathbf{k}\cdot\mathbf{p}$ method considerably increases the accuracy of the method and makes it possible to treat localized semicore states within the $\mathbf{k}\cdot\mathbf{p}$ formalism.

We have developed an approximation to the semirelativistic Foldy-Wouthuysen Hamiltonian that is applicable to such basis sets and showed its accuracy to be acceptable by testing the technique on Ag and Pb metals. The two methodological developments make it possible to perform accurate relativistic calculations of the dielectric matrix and optical properties of crystals in a wide photon-energy range including the excitations of deeply lying semicore electrons.

We have calculated *ab initio* the dielectric matrices for Pd and Pt metals within the RPA-TDLDA approach in the photon energy range up to 100 eV. We have not observed a strong effect of the microscopic fields on the optical constants of the metals below the excitation energies of the semicore states. For the semicore excitations, the nondiagonal dielectric response is essential: both in Pd and Pt the local fields cause a decrease of the absorption intensity by about 50% and dramatically change the shape of the spectra on a large energy scale to bring the theoretical curves into a good agreement with the experiment both in the peak positions and in intensity.

The absorption minima at ~ 49 eV in both metals mark the onset of the transitions from the semicore $p_{3/2}$ states. The fine structure of the $\mu(\omega)$ spectrum of Pt between 68 and 78 eV is caused by the overlapping contributions from the $5p_{1/2}$, $4f_{7/2}$, and $4f_{5/2}$ excitations. Our calculations have not revealed an inadequacy of the LDA-derived Pt $5p$ or Pd $4p$ bands to optical properties, whereas for the Pt $4f$ bands the self-energy effects not included in the calculation have been found important. The deficiency of the Pt $4f$ energies can be corrected by shifting the $4f$ band by ~ 6 eV to lower energies, the manipulations of one-electron energies being necessarily accompanied by the recalculation of the full dielectric matrix. Thereby the entire energy range up to 100 eV turns out to be well described by the one-electron theory.

ACKNOWLEDGMENTS

The authors benefited from discussions with A. Perlov and F. Starrost and are very grateful for their comments. Work was supported by the Deutsche Forschungsgemeinschaft, Forschergruppe DE 412/21. One of us (E.E.K.) acknowledges the support of the Austrian Ministry of Science under Grant No. GZ 45.446.

[1] J. H. Weaver, C. Krafka, D. W. Lynch, and E. E. Koch, *Physics Data, Optical Properties of Metals* 18-1 (H. Behrens and G. Ebel, Fachinformationszentrum Energie-Physik-Mathematik GmbH, Karlsruhe, 1981).
[2] E. E. Krasovskii and W. Schattke, Phys. Rev. B **60**, 16 251 (1999).
[3] E. E. Krasovskii and W. Schattke, Phys. Rev. B **56**, 12 874 (1997).
[4] T. L. Loucks, Phys. Rev. **139**, A1333 (1965).
[5] V. V. Nemoshkalenko, A. E. Krasovskii, V. N. Antonov, Vl. N. Antonov, U. Fleck, H. Wonn, and P. Ziesche, Phys. Status Solidi B **120**, 283 (1983).
[6] V. Theileis and H. Bross, Phys. Rev. B **62**, 13 338 (2000).
[7] D. D. Koelling and B. N. Harmon, J. Phys. C **10**, 3107 (1977).
[8] G. M. Fehrenbach and G. Schmidt, Phys. Rev. B **55**, 6666 (1997).
[9] J. C. Boettger, Phys. Rev. B **57**, 8743 (1998); J. C. Boettger, *ibid.* **62**, 7809 (2000).
[10] O. K. Andersen, Phys. Rev. B **12**, 3060 (1975).
[11] L. L. Foldy and S. A. Wouthuysen, Phys. Rev. **78**, 29 (1950).
[12] M. Douglas and N. M. Kroll, Ann. Phys. (N.Y.) **82**, 89 (1974).
[13] B. A. Hess, Phys. Rev. A **33**, 3742 (1986).
[14] H. Bross and G. M. Fehrenbach, Z. Phys. B: Condens. Matter **81**, 233 (1990).
[15] A. H. MacDonald, W. E. Pickett, and D. D. Koelling, J. Phys. C **13**, 2675 (1980).
[16] E. E. Krasovskii, F. Starrost, and W. Schattke, Phys. Rev. B **59**, 10 504 (1999).
[17] H. Ehrenreich and M. A. Cohen, Phys. Rev. **115**, 786 (1959).
[18] S. L. Adler, Phys. Rev. **126**, 413 (1962); N. Wiser, *ibid.* **129**, 62 (1962).
[19] S. P. Singhal and J. Callaway, Phys. Rev. B **14**, 2347 (1976); E. K. U. Gross and W. Kohn, Phys. Rev. Lett. **55**, 2850 (1985).
[20] R. C. Vehse, E. T. Arakawa, and M. W. Williams, Phys. Rev. B **1**, 517 (1970).
[21] J. H. Weaver, Phys. Rev. B **11**, 1416 (1975).
[22] J. H. Weaver and R. L. Benbow, Phys. Rev. B **12**, 3509 (1975).
[23] J. H. Weaver and C. G. Olson, Phys. Rev. B **14**, 3251 (1976).
[24] J. Daniels, C. v. Festenberg, H. Raether, and K. Zeppenfeld, in *Optical Constants of Solids by Electron Spectroscopy*, edited by G. Höhler, Springer Tracts in Modern Physics **54** (Springer, Berlin, 1970), p. 77; J. Daniels, Z. Phys. **227**, 234 (1969).
[25] L. Hedin and S. Lundqvist, in *Solid State Physics*, edited by F. Seitz, D. Turnbull, and H. Ehrenreich, 23 (Academic Press, New York, 1969), p. 1.
[26] G. M. Fehrenbach, Phys. Rev. B **59**, 15 085 (1999).
[27] I. I. Mazin, E. G. Maksimov, S. N. Rashkeev, and Y. A. Uspenskii, in *Metal Optics and Superconductivity* (Nova Science, New York, 1991). See also Ref. 28.
[28] E. G. Maksimov, I. I. Mazin, S. N. Rashkeev, and Y. A. Uspenskii, J. Phys. F: Met. Phys. **18**, 833 (1988).
[29] The comparison with the EELS experiment in Refs. 26 and 28 is misleading: the dotted curve in Fig. 1 of Ref. 26 and the dashed curve in Fig. 4 of Ref. 28 are identical and are in both papers referred to as the experiment of Daniels [24]. In fact, the two curves do not correspond to the curve presented in Ref. 24.
[30] R. Haensel, K. Radler, B. Sonntag, and C. Kunz, Solid State Commun. **7**, 1495 (1969).
[31] R. E. Dietz, E. G. McRae, and J. H. Weaver, Phys. Rev. B **21**, 2229 (1980).
[32] G. K. Wertheim and L. R. Walker, J. Phys. F: Met. Phys. **6**, 2297 (1976).
[33] G. K. Wertheim (unpublished); Data quoted by Dietz *et al.* (Ref. 31).
[34] A. R. Williams and U. von Barth in *Theory of the Inhomogeneous Electron Gas*, edited by S. Lundqvist and N. H. March (Plenum Press, New York, 1983), p. 189.